Suplemento de la Revista Mexicana de Física **4** 021111 (2023) 1–9

Study of cLFV with $\ell_i \ell_j \gamma\gamma$ effective vertex

F. Fortuna

Centro de Investigación y de Estudios Avanzados,
Apartado Postal 14-740, 07000, Ciudad de México, México.

Received 15 May 2023; accepted 19 June 2023

In this work we analyze cLFV processes using a low-energy EFT that induces the effective interaction between two charged leptons of different flavor and two photons. We compute $\ell_i \to \ell_j \gamma$, $\ell_i \to \ell_j \gamma\gamma$ decays and $\ell_i \to \ell_j$ conversion in nuclei. We derived indirect upper limits on the double photon decays, which turned out to be below current experimental bounds. Our prediction for $\ell \to \tau$ conversion in nuclei is below the expected sensitivity of the NA64 experiment.

Keywords: Charged lepton flavor violation; effective theory.

DOI: https://doi.org/10.31349/SuplRevMexFis.4.021111

1. Introduction

In the SM, lepton flavor is conserved (which also holds in its minimally extended version, at the tree level, for the charged-lepton sector), therefore, any measurable signal of a process with lepton flavor violation in the charged sector (cLFV) would be a sign of new physics.

In this work we analyze the $\ell_i \ell_j \gamma\gamma$ effective interactions, in particular we study the cLFV decays of leptons to two photons, $\ell_i \to \ell_j \gamma\gamma$ [1–3], and consider its theoretical correlation with the $\ell_i \to \ell_j \gamma$ decays, which have been explored in more detail, both theoretically and experimentally than the former processes, specially decays involving the τ lepton [4–8].

In Table I, we show the current upper limits from direct experimental searches for both single and double photon decays. Notice that the upper bounds for the single photon processes are several orders of magnitude more stringent than for the double photon processes, and this difference is even larger in the τ sector. In fact, no direct experimental search exists for $\tau \to e\gamma\gamma$.

Any new physics scenario generating $\ell_i \to \ell_j \gamma\gamma$ would also generate a (model-dependent) contribution to $\ell_i \to \ell_j \gamma$ at the loop level. We analyzed this correlation within an EFT framework and derive general, model-independent indirect limits on the $\ell_i \to \ell_j \gamma\gamma$ decays, which turn out to be below current experimental bounds.

On the other hand, in the literature there are plenty of models proposed to describe the cLFV processes. If cLFV is discovered, observations or experimental bounds from multiple independent processes would be helpful to discriminate among those models.

A well-motivated scenario to study cLFV interactions is the $\ell_i - \ell_j$ conversion in nuclei. Currently the strongest limit on $\mu - e$ conversion in nuclei was set by Sindrum II [14]:

$$\mathcal{B}_{\mu e}^{Au} = \frac{\Gamma(\mu^- \mathrm{Au} \to e^- \mathrm{Au})}{\Gamma_{\mathrm{capture}}(\mu^- \mathrm{Au})} < 7 \times 10^{-13}, \quad 90\%\mathrm{C.L.}$$

In general, cLFV processes involving the τ lepton, imply a greater experimental challenge. In fact, there are still no experimental limits for nuclei transitions involving τ's; however, at the CERN SPS, the NA64 experiment plans a search for $\ell \to \tau$ conversion in nuclei [15]. The conversion is expected to occur by deep inelastic scattering (DIS) of the lepton on the nucleus, as shown in Fig. 1. Using the stringent limits that we derived from $\ell_i \to \ell_j \gamma$, we compute upper bounds on the $\ell_i \to \ell_j$ transitions in nuclei with an EFT approach.

This work is organized as follows: in Sec. 2 we present the Lagrangian that we employ [2]. Then, in Sec. 3 we study the correlation between the single and double photon decays, and derived indirect limits on the latter. After that, in Secs. 4 and 5 we compute $\ell \to \tau$ and $\mu \to e$ conversion in nuclei, respectively. Finally, we give our conclusions in Sec. 6.

TABLE I. Experimental upper bounds on the rates of the $\ell_i \to \ell_j \gamma(\gamma)$ decays.

Decay Mode	Current upper limit on BR (90%CL)	
$\mu \to e\gamma$	4.2×10^{-13}	MEG (2016) [9]
$\mu \to e\gamma\gamma$	7.2×10^{-11}	Crystal Box (1986) [10]
$\tau \to e\gamma$	3.3×10^{-8}	BaBar (2010) [11]
$\tau \to \mu\gamma$	4.2×10^{-8}	Belle (2021) [12]
$\tau \to \mu\gamma\gamma$	1.5×10^{-4}	ATLAS (2017) [13]

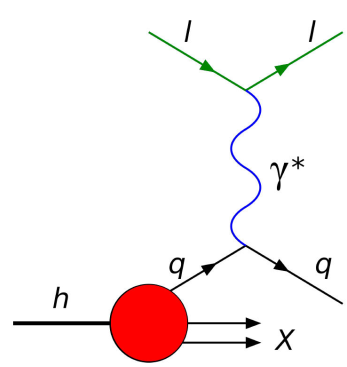

FIGURE 1. Deep inelastic scattering of a lepton (l) on a hadron (h).

2. Effective operators

The effective $\ell_i\ell_j\gamma\gamma$ vertex is generated by the following low-energy, dimension-7 operators [2]

$$\begin{aligned}\mathcal{L}_{\text{Int}} &= \left(G^{ij}_{SR}\bar{\ell}_{L_i}\ell_{R_j} + G^{ij}_{SL}\bar{\ell}_{R_i}\ell_{L_j}\right)F_{\mu\nu}F^{\mu\nu}\\ &+ \left(\tilde{G}^{ij}_{SR}\bar{\ell}_{L_i}\ell_{R_j} + \tilde{G}^{ij}_{SL}\bar{\ell}_{R_i}\ell_{L_j}\right)\tilde{F}_{\mu\nu}F^{\mu\nu}\\ &+ \left(G^{ij}_{VL}\bar{\ell}_{L_i}\gamma^\sigma\ell_{L_j} + G^{ij}_{VR}\bar{\ell}_{R_i}\gamma^\sigma\ell_{R_j}\right)F^{\mu\nu}\partial_\nu F_{\mu\sigma}\\ &+ \left(\tilde{G}^{ij}_{VL}\bar{\ell}_{L_i}\gamma^\sigma\ell_{L_j} + \tilde{G}^{ij}_{VR}\bar{\ell}_{R_i}\gamma^\sigma\ell_{R_j}\right)F^{\mu\nu}\partial_\nu \tilde{F}_{\mu\sigma}\\ &+ h.c.\,, \end{aligned} \tag{1}$$

where i, j are generation indices, the subscripts $L(R)$ indicate the chirality of the lepton and $\tilde{F}_{\mu\nu} = (1/2)\epsilon_{\mu\nu\sigma\lambda}F^{\sigma\lambda}$ is the dual tensor.

However, the effect of the dimension-8 operators is firstly suppressed by a higher power of the cut-off scale of the EFT, and secondly, due to a helicity flip is also suppressed by the mass of the decaying lepton, so we will neglect them in what follows.

On the other hand, the effective $\ell_i\ell_j\gamma$ vertex is generated by the following dimension-5 operators:

$$\begin{aligned}\mathcal{L}_{\text{dim-5}} &= D^{ij}_R\,\bar{\ell}_{L_i}\sigma_{\mu\nu}\ell_{R_j}F^{\mu\nu} + D^{ij}_L\,\bar{\ell}_{R_i}\sigma_{\mu\nu}\ell_{L_j}F^{\mu\nu}\\ &+ h.c. \end{aligned} \tag{2}$$

3. Indirect limits on $\ell_i \to \ell_j\gamma\gamma$ from $\ell_i \to \ell_j\gamma$

Let us first consider the scenario of our interest in which dimension-5 operators are suppressed —by a symmetry in the UV complete theory—, then the contributions generated by the dimension-7 operators in Eq. (1) dominate. The decay $\ell_i \to \ell_j\gamma\gamma$ is generated at tree level with a total decay rate

$$\Gamma(\ell_i \to \ell_j\gamma\gamma) = \frac{|G_{ij}|^2}{3840\pi^3}\,m_i^7\,, \tag{3}$$

where we have neglected the mass of the final lepton, and

$$|G_{ij}|^2 = |G^{ij}_{SL}|^2 + |G^{ij}_{SR}|^2 + |\tilde{G}^{ij}_{SL}|^2 + |\tilde{G}^{ij}_{SR}|^2. \tag{4}$$

In this scenario, the decay $\ell_i \to \ell_j\gamma$ is generated at the one loop level, see Fig. 2, and keeping only the leading terms, one obtains the approximate decay rate:

$$\Gamma(\ell_i \to \ell_j\gamma) \sim \frac{\alpha\,|G_{ij}|^2}{256\,\pi^4}\,m_i^7\,\log^2\left(\frac{\Lambda^2}{m_i^2}\right)\,, \tag{5}$$

where Λ stands for the EFT cut-off energy scale. We then found an approximate correlation between the rates in Eqs. (3) and (5)

$$\Gamma(\ell_i \to \ell_j\gamma) \sim \frac{15\alpha}{\pi}\,\log^2\left(\frac{\Lambda^2}{m_i^2}\right)\,\Gamma(\ell_i \to \ell_j\gamma\gamma)\,, \tag{6}$$

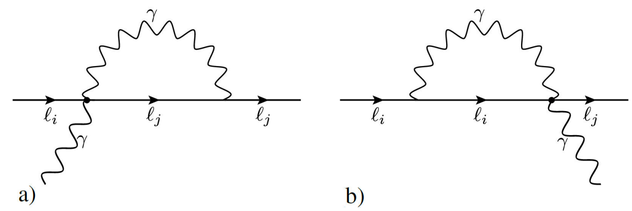

FIGURE 2. One loop contributions to $\ell_i \to \ell_j\gamma$.

and using the experimental upper bounds on $\ell_i \to \ell_j\gamma$ from Table I, we derived indirect upper limits on $\ell_i \to \ell_j\gamma\gamma$ [1]:

$$\begin{aligned}\text{BR}(\mu \to e\gamma\gamma) &\lesssim 6.4\times 10^{-14}\left[1{+}0.15\log\tfrac{\Lambda}{100\,\text{GeV}}\right]^{-2},\\ \text{BR}(\tau \to e\gamma\gamma) &\lesssim 1.5\times 10^{-8}\ \left[1{+}0.25\log\tfrac{\Lambda}{100\,\text{GeV}}\right]^{-2},\\ \text{BR}(\tau \to \mu\gamma\gamma) &\lesssim 1.9\times 10^{-8}\ \left[1{+}0.25\log\tfrac{\Lambda}{100\,\text{GeV}}\right]^{-2}, \end{aligned} \tag{7}$$

which have a mild sensitivity to the cut-off energy scale.

Let us now analyze the scenario in which dimension-5 operators yield the leading contribution. The $\ell_i \to \ell_j\gamma$ decay is induced at tree level, with a total decay rate

$$\Gamma(\ell_i \to \ell_j\gamma) = \frac{m_i^3}{4\pi}\left(\left|D^{ij}_R\right|^2 + \left|D^{ij}_L\right|^2\right)\,. \tag{8}$$

Clearly these dimension-5 operators may also induce the $\ell_i \to \ell_j\gamma\gamma$ decay, whose decay rate is given by

$$\Gamma(\ell_i \to \ell_j\gamma\gamma) = \frac{\alpha\,m_i^3}{48\pi^2}\left(|D^{ij}_R|^2 + |D^{ij}_L|^2\right)\lambda\left(\tfrac{E^{\text{cut}}_\gamma}{m_i}\right)\,, \tag{9}$$

with E^{cut}_γ an energy cut-off introduced to regularize the collinear and infrared divergences in the rate, and

$$\begin{aligned}\lambda(x) &\simeq 6 + 2\pi^2 + 6\log^2 2 + 21\log(2x) + 6\log(x)\,\log(4x)\\ &+ 18x\big(2\log(2x)+1\big) + 6x^2\big(8\log(2x) - 29\big)\\ &+ \mathcal{O}(x^3)\,. \end{aligned} \tag{10}$$

We may again find a correlation between the rates in Eqs. (8) and (9),

$$\Gamma(\ell_i \to \ell_j\gamma\gamma) = \frac{\alpha}{12\pi}\,\lambda\left(\frac{E^{\text{cut}}_\gamma}{m_i}\right)\,\Gamma(\ell_i \to \ell_j\gamma)\,. \tag{11}$$

Imposing $E^{\text{cut}}_\gamma = 7\,(50)$ MeV for $\mu\,(\tau)$ decays, and using the upper limits on the rates for $\ell_i \to \ell_j\gamma$, we found the following indirect bounds:

$$\begin{aligned}\text{BR}(\mu \to e\gamma\gamma) &\lesssim 2\times 10^{-16}\,,\\ \text{BR}(\tau \to e\gamma\gamma) &\lesssim 8\times 10^{-11}\,,\\ \text{BR}(\tau \to \mu\gamma\gamma) &\lesssim 1\times 10^{-10}\,. \end{aligned} \tag{12}$$

By comparing the indirect limits in Eqs. (7) and (12) we see that the observable with two photons, $\ell_i \to \ell_j\gamma\gamma$

is favored when dimension-7 operators dominate, while it is very suppressed when the leading contribution is due to dimension-5 operators.

Notice that our indirect upper limits are significantly more stringent than the current experimental bounds (see Table I), regardless of the underlying physics generating the process $\ell_i \to \ell_j \gamma\gamma$.

Specifically, focusing on our indirect limits from dimension-7 operators, the upper bound on $\tau \to \mu\gamma\gamma$ is about four orders of magnitude stronger than the experimental search by ATLAS and the limit on $\mu \to e\gamma\gamma$ is about three orders of magnitude stronger than the experimental bound using the Crystal Box detector.

We want to highlight that our results in Eq. (7) show that $\tau \to \ell\gamma\gamma$ decays may be at reach of future experiments [16] and therefore motivate a dedicated experimental search. Also, future foreseeable sensitivities of Belle II searching for $\tau \to \ell\gamma$ and MEG II for $\mu \to e\gamma$ will improve our indirect bounds by about an order of magnitude.

Belle II might reach a sensitivity of $\mathcal{O}(10^{-9})$ for the branching ratios $\tau \to \ell\gamma\gamma$, assuming that it could achieve the same sensitivity for single and double photon processes (as occurred for μ decays in the Crystal Box Detector [17]). In this case, Belle II will probe unexplored parameter space of the dimension-7 operators, and could possibly observe the decay $\tau \to \ell\gamma\gamma$, finding evidence of cLFV.

Directly from Eq. (5), using the experimental limits on $\ell_i \to \ell_j\gamma$, we can derive limits on the G_{ij} effective couplings that we will use in the following

$$
\begin{aligned}
|G_{\tau e}| &\leq 8.4 \times 10^{-9} \left[1 + 0.25 \log \frac{\Lambda}{100\text{ GeV}}\right]^{-1} \text{GeV}^{-3}\,, \\
|G_{\tau \mu}| &\leq 9.5 \times 10^{-9} \left[1 + 0.25 \log \frac{\Lambda}{100\text{ GeV}}\right]^{-1} \text{GeV}^{-3}\,, \\
|G_{\mu e}| &\leq 1.2 \times 10^{-10} \left[1 + 0.15 \log \frac{\Lambda}{100\text{ GeV}}\right]^{-1} \text{GeV}^{-3}\,.
\end{aligned}
\tag{13}
$$

4. $\ell \to \tau$ conversion in nuclei

In the $\ell_i \to \tau$ experiments an electron or muon beam hits a fixed-target nucleus, if the beam energy is high enough, the leptons interact with the partons, *i.e.*, quarks and gluons, by breaking the hadronic structure of the nucleons within the nucleus [15].

We will focus on inclusive processes, *i.e.*, $\ell_i + \mathcal{N}(A,Z) \to \tau + X$, whose products of interaction are a τ lepton plus any hadrons, and where we do not have information about X.

The low-energy non-perturbative QCD effects heavily influence the dynamics of the interacting parton living in the hadronic environment of the nucleus. This non-perturbative behavior is encoded in the so-called parton distribution functions (PDFs). We are interested in calculating the total cross section of the aforementioned process, and using QCD factorization theorems, we can obtain it by computing the convolution of the non-perturbative PDFs (f) with the perturbative cross-section ($\hat{\sigma}$)

$$\sigma_{\ell\to\tau} = f \otimes \hat{\sigma}. \tag{14}$$

Given that we compute the perturbative cross-section within the EFT framework, this calculation is valid up to a certain scale, the characteristic energy scale, usually taken as $Q^2 = -q^2$, being q^2 the transferred momentum of the system. Both the PDFs and the perturbative cross-sections are functions of Q^2 and, in addition, the PDFs are also characterized through the Lorentz invariant quantity, ξ, the fraction of the nucleus momentum carried by the interacting parton. Therefore, we express the PDFs as well as the perturbative cross-section as functions of the two discussed invariant quantities

$$\sigma_{\ell\to\tau} = \hat{\sigma}(\xi, Q^2) \otimes f(\xi, Q^2). \tag{15}$$

The PDFs dependence on the momentum fraction ξ is directly extracted from the data, while to describe their evolution in terms of Q^2, the DGLAP evolution equations are used [18–20]. Since, in our case, we are dealing with heavy nuclei instead of free nucleons, it is more suitable to use the nuclear parton distribution functions (nPDFs) to describe the $\ell \to \tau$ conversion in nuclei. For this calculation we use the nCTEQ15-np fit of the nPDFs, provided by the group around the nCTEQ15 project [21], and incorporated within the `ManeParse Mathematica package` [22].

Using the dimension-7 operators in the Lagrangian in Eq. (1), we compute the following contributions to the perturbative cross-section:

(a) $\ell_i q \to \tau q$ process (see Fig. 3), that involves a loop with a quark and two photons.

(b) $\ell_i \bar{q} \to \tau \bar{q}$, that is the same process as in (a), but with antiquarks. The perturbative cross sections are different than those involving quarks, and also the non-perturbative behavior of antiquarks inside the nucleons is not the same as their opposite-charged partners.

There is a possible additional contribution to our cross section of interest, by the $\ell_i g \to \tau g$: starting from the diagram in Fig. 18, if we close the quark lines in an additional loop and we couple the initial and final gluons to it. However, it would be generated at two loop level by our dimension-7 operators and therefore we do not include it.

Considering the previously mentioned contributions to the perturbative cross-section, we derived the following matrix element squared, as a function of Q^2 and ξ

$$\overline{|\mathcal{M}_{qq}(\xi,Q^2)|^2} = 2e^4\left(|G_{LR}^{\tau\ell}|^2+|G_{RL}^{\tau\ell}|^2\right)\left[\left(m_\ell^2+m_\tau^2+Q^2\right)\left(\left(m_i+\xi M\right)^2+Q^2\right)\right]\Gamma_{qq}(\xi,Q^2)$$
$$+\frac{1}{2}e^4\left(|\tilde{G}_{LR}^{\tau\ell}|^2+|\tilde{G}_{RL}^{\tau\ell}|^2\right)\left[\left(m_\ell^2+m_\tau^2+Q^2\right)\left(\left(m_i-\xi M\right)^2+Q^2\right)\right]\tilde{\Gamma}_{qq}(\xi,Q^2)\,, \qquad (16)$$

where $\Gamma(\xi,Q^2)$ and $\tilde{\Gamma}(\xi,Q^2)$ are functions resulting from the calculation of the loops (see Fig. 3), and are shown Ref. [23].

Analogous expressions are obtained for the process with antiquarks except that the corresponding "$\Gamma(\xi,Q^2)$" functions are different. The interference term between operators with and without dual tensor vanishes, while we neglect the interference between left and right operators because is chirality suppressed.

From the matrix element squared in Eq. (16), the perturbative unpolarized differential cross sections can be computed as a function of ξ and Q^2,

$$\frac{d\hat{\sigma}(\ell\, q_i(\xi P)\to\tau\, q_i)}{d\xi dQ^2} = \frac{1}{16\pi\lambda(s(\xi),m_\ell^2,m_i^2)}\overline{|\mathcal{M}_{qq}(\xi,Q^2)|^2}\,,$$
$$\frac{d\hat{\sigma}(\ell\, \bar{q}_i(\xi P)\to\tau\, \bar{q}_i)}{d\xi dQ^2} = \frac{1}{16\pi\lambda(s(\xi),m_\ell^2,m_i^2)}\overline{|\mathcal{M}_{\bar{q}\bar{q}}(\xi,Q^2)|^2}\,, \qquad (17)$$

where i labels the quark flavor, $p_i=\xi P$ is the momentum of the interacting parton, P the nucleus total momentum, and we have defined $m_i^2=\xi^2M^2$, being M the nucleus mass; $\lambda(s(\xi),m_\ell^2,m_i^2)$ stands for the usual Källén function. Finally, at leading order (LO) in the QCD formalism, the total cross-section reads

$$\sigma(\ell N(P)\to\tau X) = \sum_i \int_{\xi_{\min}}^{1}\int_{Q_-^2(\xi)}^{Q_+^2(\xi)} d\xi dQ^2\left\{\frac{d\hat{\sigma}(\ell\, q_i(\xi P)\to\tau\, q_i)}{d\xi\, dQ^2}f_{q_i}(\xi,Q^2)+\frac{d\hat{\sigma}(\ell\, \bar{q}_i(\xi P)\to\tau\, \bar{q}_i)}{d\xi dQ^2}f_{\bar{q}_i}(\xi,Q^2)\right\}\,,$$

with $f_{q_i}(\xi,Q^2)$ and $f_{\bar{q}_i}(\xi,Q^2)$ the quark and antiquark nPDFs, respectively. In appendix E of Ref. [24] the integration limits can be found.

At this point, we can compute the ratio between the conversion probabilities

$$\mathcal{R}_{\tau\ell} = \frac{\sigma(\ell\mathcal{N}\to\tau X)}{\sigma(\ell\mathcal{N}\to\ell X)}\,, \qquad (18)$$

that is our quantity of interest since we can compare our prediction with the expected sensitivity of the NA64 experiment, of $\mathcal{R}_{\tau\ell}\sim[10^{-13},10^{-12}]$ [15]. The denominator in Eq. (18) is the lepton bremsstrahlung on nuclei, that is the dominant contribution to the inclusive $\ell+\mathcal{N}$ process, and we took it from Ref. [15].

We set three benchmark scenarios for our numerical analysis

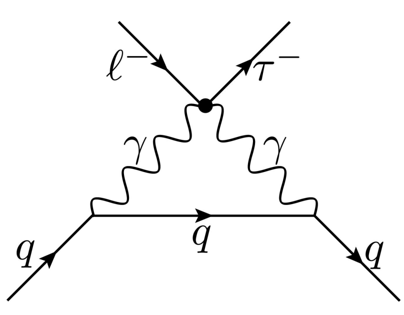

FIGURE 3. One loop contribution to $\ell_i q\to\tau q$, with $\ell_i=e,\mu$.

$$(i)\ |G_{\tau\ell}|^2 = |G_{SR}^{\tau\ell}|^2+|G_{SL}^{\tau\ell}|^2 = |\tilde{G}_{SR}^{\tau\ell}|^2+|\tilde{G}_{SL}^{\tau\ell}|^2\,,$$
$$(ii)\ |G_{\tau\ell}|^2 = |G_{SR}^{\tau\ell}|^2+|G_{SL}^{\tau\ell}|^2;\ \tilde{G}_{SR}^{\tau\ell}=\tilde{G}_{SL}^{\tau\ell}=0\,,$$
$$(iii)\ |G_{\tau\ell}|^2 = |\tilde{G}_{SR}^{\tau\ell}|^2+|\tilde{G}_{SL}^{\tau\ell}|^2;\ G_{SR}^{\tau\ell}=G_{SL}^{\tau\ell}=0\,, \qquad (19)$$

taking the upper limit on $|G_{\tau\ell}|^2$ from Eqs. (13)[i].

According to the prospects of the NA64 experiment [15], we use $E_e=100$ GeV and $E_\mu=150$ GeV in our analysis for the energies of the incident lepton beams[ii], as well as two specific nuclei, Fe(56,26) and Pb(208,82).

We evaluate the integral in Eq. (18) in the three benchmark scenarios for $|G_{\tau\ell}|^2$ described above to obtain the $\mathcal{R}_{\tau\ell}$ ratio in the different channels explored. Our results are shown in Fig. 4, and are compared with the expected sensitivity of the NA64 experiment, which is displayed as a gray area.

In fact, we also want to highlight the impact on the ratios $\mathcal{R}_{\tau\ell}$ due to the stringent indirect limits on $|G_{\tau\ell}|$ derived in Eq. (13). If we compute limits on these effective couplings $|G_{\tau\ell}|$ directly from the tree level $\ell_i\to\ell_j\gamma\gamma$ decays —whose decay rates are shown in Eq. (3)—, and using the direct limits in Table I, we obtain the ratios $\mathcal{R}_{\tau\ell}$ displayed in Fig. 5 —where the expected sensitivity of the NA64 experiment is also shown.

We see in Fig. 5 that using the direct limits on the $\ell_i\to\ell_j\gamma\gamma$ one might naively expect that the $\mu\mathrm{Fe}\to\tau X$ and $\mu\mathrm{Pb}\to\tau X$ could be within the reach of the NA64 experiment. However, we see in Fig. 4 that this is not the case,

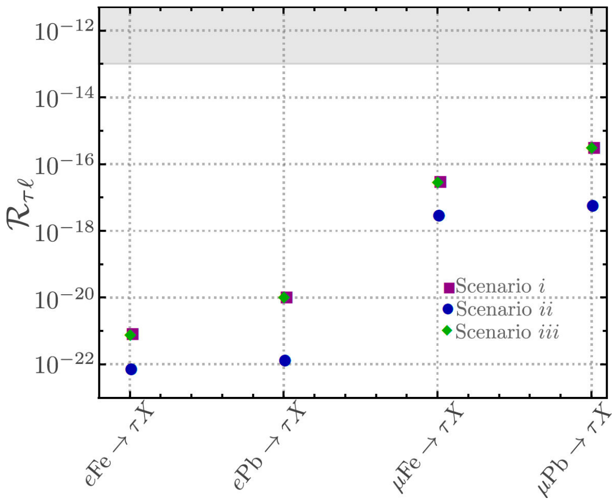

FIGURE 4. Upper limits for the ratios $\mathcal{R}_{\tau\ell}$, in Eq. (18). The different scenarios are described in Eq. (19) and the values of $|G_{\tau\ell}|$ come from the Eq. (13), assuming $\Lambda = 100$ GeV.

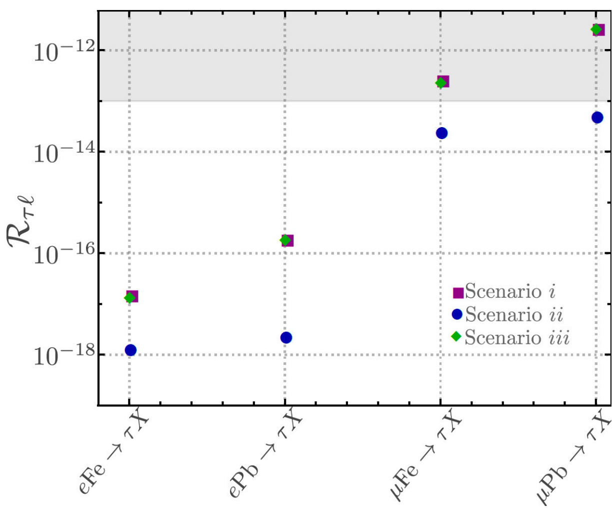

FIGURE 5. Upper limits for the ratios $\mathcal{R}_{\tau\ell}$, in Eq. (18), obtained for $\ell \to \tau$ conversion in nuclei, compared to the NA64 expected sensitivity (gray band). The different scenarios are described in Eq. (19).

because our predicted ratios $\mathcal{R}_{\tau\ell}$ are several orders of magnitude below the expected sensitivity of the experiment.

Notice that the muon channels have larger predicted ratios $\mathcal{R}_{\tau\ell}$ than the electron channels. In Ref. [24] Husek *et al.* also obtained larger results for $\mu \to \tau$ than for $e \to \tau$ transitions, and they explained that the reason is that the normalization channel (the bremsstrahlung cross section) in the ratio $\mathcal{R}_{\tau\ell}$ is much smaller for muons than for electrons.

However, we obtain better results for the $\mu \to \tau$ conversion in lead than in iron, while Husek *et al.* found the opposite. In case of an eventual observation, these different results could help to probe the type of new physics inducing these transitions.

Using SMEFT would be more appropriate to study $\ell \to \tau$ conversions in nuclei, where our low-energy effective operators become $D = 8$ operators (to generate $SU(2) \times U(1)$ invariants), and there would be additional dimension-8 contributions. However, operators involving Z bosons instead of photons would be negligible with respect to the di-photon ones. Besides, we do not expect the (soft) running of the Wilson coefficient to alter our results. On the other hand, we see from Fig. 4 that our predictions for $\ell \to \tau$ conversion in nuclei are not at reach of future foreseen experiments and the complete calculation of these processes with dimension-8 operators is beyond our scope.

5. $\mu \to e$ conversion in nuclei

Davidson *et al.* [3] analyzed $\mu \to e$ conversions using the dimension-7 operators. They found that the limit on $|G_{\mu e}|$ from $\mu \to e$ conversion in nuclei is about one order of magnitude more stringent than the limit from the $\mu \to e\gamma\gamma$ decay.

However, the indirect limits we derived in Sec. 3 from $\ell_i \to \ell_j\gamma$, are currently the most stringent bounds on the $|G_{ij}|$ effective couplings. In this section we will use our constraint on $|G_{\mu e}|$, in Eq. (13), to compute upper limits on $\mu \to e$ conversion in nuclei.

The $\mu \to e$ conversion in nuclei is explained in detail in Ref. [3]. Here we will only sketch the main contributions. Notice that the $F_{\mu\nu}\tilde{F}^{\mu\nu}$ operators are proportional to $\vec{E}\cdot\vec{B}$, which is negligibly small in the nucleus, and therefore we will neglect them in the calculation.

In Ref. [3], the authors explain that the $\mu \to e$ conversion in nuclei has two main contributions. First the interaction of the leptons with the classical electromagnetic field, that arises at momentum transfers $\sim m_\mu$ for a contact $\mu e\gamma\gamma$ interaction. Secondly, there is a surprisingly large "short distance" loop interaction of individual protons with two photons; stemming from the loop mixing of the $\bar{e}\mu F_{\mu\nu}F^{\mu\nu}$ operator into the scalar proton operator, $\mathcal{O}_{S,X} = (\bar{e}P_X\mu)(\bar{p}p)$ (X labeling the chirality). The naive expectation of a loop suppression is overcompensated by energy ratios, numerical factors and overlap integrals. Thus, we have [3]

$$\mathrm{BR}(\mu A\to eA)=\frac{4m_\mu^5}{\Gamma_{\mathrm{cap}}}|G_{\mu e}|^2\left(m_\mu F_A+\frac{18\alpha m_p}{\pi}S_A^{(p)}\right)^2. \tag{20}$$

where $S_A^{(N)}$ and F_A are overlap integrals that can be found in [3, 25], respectively, and Γ_{cap} is the muon capture rate on nucleus A [26].

Using the upper limit derived for $|G_{\mu e}|$, in Eq. (13), and assuming conservatively that $\Lambda = 100$ GeV, we find upper limits on the $\mathrm{BR}(\mu\mathrm{A} \to \mathrm{eA})$, with A= ^{197}Au, ^{27}Al

$$\mathrm{BR}(\mu\,\mathrm{Au}\to\mathrm{e\,Au}) \le 2.7\times 10^{-13}\,,$$
$$\mathrm{BR}(\mu\,\mathrm{Al}\to\mathrm{e\,Al}) \le 6.9\times 10^{-13}\,. \tag{21}$$

Comparing the upper limit on $\mathrm{BR}(\mu\mathrm{Au}\to\mathrm{eAu})$ by the SINDRUM II experiment [14] with the value obtained in Eq. (21), we see that the latter is slightly stronger.

In Eq. (21) we add our prediction for the $\mu \to e$ conversion in aluminum since the upcoming Mu2e [27] and COMET [28] experiments plan to start with an aluminum target.

6. Discussion and conclusions

In this work we first derive indirect upper limits on the $\ell \to \tau\gamma\gamma$ decays. We show that, in scenarios where the leading contribution is generated by dimension-7 operators, the rare $\ell_i \to \ell_j\gamma\gamma$ decays can be enhanced and even been within the reach of the Belle II experiment.

Concerning the $\mu - e$ sector, any improvement on $\mu \to e$ conversion in nuclei or $\mu \to e\gamma$, will enhance the sensitivity to the effective coupling $G_{\mu e}$.

The target sensitivity of the MEG II experiment for $\mu \to e\gamma$ will be $\mathcal{O}(10^{-14})$ [29], and in the long term, it is widely expected that $\mu \to e$ conversion in nuclei experiments will reach sensitivities $\mathcal{O}(10^{-18})$ [27,30,31] or lower. Therefore, in the future the more stringent constraints on the low-energy dimension-7 operators, in the $\mu - e$ sector, will be provided by $\mu \to e$ conversion in nuclei.

Concerning the τ sector, by comparing Figs. 4 and 5 we see that the big improvement in $|G_{\tau\ell}|$ from $\tau \to \ell\gamma$, precludes the early observation by the NA64 experiment of $\ell \to \tau$ conversion in nuclei induced by the $\ell_i\ell_j\gamma\gamma$ effective interactions. However, future foreseen experiments such as the electron-ion collider (EIC) [32], the muon collider [33], circular colliders as LHeC [34] or the ILC [35] might search for this conversion in addition to the NA64 experiment. Another way to probe our effective di-photon vertex, $\ell_i\ell_j\gamma\gamma$, is in an electron-positron collider through the $e^+e^- \to \gamma^* \to \ell_i^+\ell_j^-\gamma$ process, with $\ell_i \neq \ell_j$, for $\sqrt{s} \ll m_Z$. However several difficulties arises, first it is suppressed by an additional factor of α from the $e^+e^- \to \gamma^*$ vertex besides the effective dimension-7 vertex. On the other hand, it would not be possible to distinguish between the effective vertex $\ell_i\ell_j\gamma$ plus a photon of final state radiation (photon coupled to any of the final leptons) from our effective vertex with two leptons and two photons.

Appendix

A. Functions from the loops evaluation in $\ell \to \tau$ conversion in nuclei

Here we display the relevant functions that appear in the matrix element squared in Eq. (16), which result from the evaluation of the loop in Fig. 5.

In particular, we define

$$\begin{aligned}
\Gamma_{qq}(\xi, Q^2) &= \frac{1}{64\pi^4}|\mathrm{F1}(\xi, Q^2)|^2\,,\\
\tilde{\Gamma}_{qq}(\xi, Q^2) &= \frac{1}{64\pi^4}|\mathrm{F2}(\xi, Q^2)|^2\,,\\
\Gamma_{\bar{q}\bar{q}}(\xi, Q^2) &= \frac{1}{64\pi^4}|\mathrm{F3}(\xi, Q^2)|^2\,,\\
\tilde{\Gamma}_{\bar{q}\bar{q}}(\xi, Q^2) &= \frac{1}{64\pi^4}|\mathrm{F4}(\xi, Q^2)|^2\,,
\end{aligned} \tag{A.1}$$

with

$$\begin{aligned}
\mathrm{F1} = {} & 2\big[m(Q^2) + M\xi\big]\mathbf{B}_0(M^2\xi^2; m(Q^2), 0) + 2\big[m(Q^2) + m_i\big]\mathbf{B}_0(m_i^2; m(Q^2), 0)\\
& + 2\big[m(Q^2) - m_i\big]\mathbf{B}_0(-Q^2; 0, 0) + 2M\xi\,\mathbf{B}_1(M^2\xi^2; m(Q^2), 0) + 2\big[M\xi - m_i\big]\mathbf{B}_1(-Q^2; 0, 0)\\
& + 2m_i\,\mathbf{B}_1(m_i^2; m(Q^2), 0) + 2\big[m^3(Q^2) + Mm_i\,m(Q^2)\xi - M^2m_i\xi^2 + m(Q^2)Q^2 - Mm_i^2\xi\big]\\
& \mathbf{C}_0(m_i^2, -Q^2, M^2\xi^2; m(Q^2), 0, 0) + 2\big[m^2(Q^2) - m_i^2 + m_im(Q^2) - m_iM\xi - M^2\xi^2 + Mm(Q^2)\xi\big]\\
& \big(M\xi\,\mathbf{C}_2(m_i^2, -Q^2, M^2\xi^2; m(Q^2), 0, 0) + m_i\,\mathbf{C}_1(m_i^2, -Q^2, M^2\xi^2; m(Q^2), 0, 0)\big)\\
& + m_i - 4m(Q^2) + M\xi\,.
\end{aligned} \tag{A.2}$$

$$\begin{aligned}
\mathrm{F2} = {} & -2i\Big(2\big[M\xi + m(Q^2)\big]\mathbf{B}_0(M^2\xi^2; m(Q^2), 0) + 2\big[m_i + m(Q^2)\big]\mathbf{B}_0(m_i^2; m(Q^2), 0)\\
& + 2\big[M\xi + m_i - 2m(Q^2)\big]\mathbf{B}_0(-Q^2; 0, 0) + 2M\xi\,\mathbf{B}_1(M^2\xi^2; m(Q^2), 0) + 2m_i\,\mathbf{B}_1(m_i^2; m(Q^2), 0)\\
& + 2\big[m_im^2(Q^2) - 2m^3(Q^2) + Mm^2(Q^2)\xi - Mm_i^2\xi - M^2m_i\xi^2 + 2Mm_im(Q^2) + m(Q^2)Q^2\big]\\
& \mathbf{C}_0(m_i^2, -Q^2, M^2\xi^2; m(Q^2), 0, 0) + 2\big[m_i^2 - 2m_im(Q^2) - M^2\xi^2 + 2Mm(Q^2)\xi\big]\\
& \big(m_i\,\mathbf{C}_1(m_i^2, -Q^2, M^2\xi^2; m(Q^2), 0, 0) - M\xi\,\mathbf{C}_2(m_i^2, -Q^2, M^2\xi^2; m(Q^2), 0, 0)\big) - 3(m_i + M\xi)\Big).
\end{aligned} \tag{A.3}$$

$$\begin{aligned}
\mathrm{F3} =\, & 2\big[m(Q^2) - M\xi\big]\mathbf{B}_0(M^2\xi^2; m(Q^2), 0) + 2\big[m(Q^2) - m_i\big]\mathbf{B}_0(m_i^2; m(Q^2), 0) \\
& + 2\big[m(Q^2) + m_i\big]\mathbf{B}_0(-Q^2; 0, 0) - 2M\xi\,\mathbf{B}_1(M^2\xi^2; m(Q^2), 0) - 2m_i\,\mathbf{B}_1(m_i^2; m(Q^2), 0) \\
& + 2\big[m_i - M\xi\big]\mathbf{B}_1(-Q^2; 0, 0) + 2\big[M^2\xi^2 + m_i\big(M\xi + m(Q^2)\big) + Mm(Q^2)\xi + m_i^2 - m^2(Q^2)\big] \\
& \big(M\xi\,\mathbf{C}_2(m_i^2, -Q^2, M^2\xi^2; m(Q^2), 0, 0) + m_i\,\mathbf{C}_1(m_i^2, -Q^2, M^2\xi^2; m(Q^2), 0, 0)\big) \\
& + 2\big[m^3(Q^2) + Mm_i m(Q^2)\xi + M^2 m_i\xi^2 + m(Q^2)Q^2 + Mm_i^2\xi\big]\mathbf{C}_0(m_i^2, -Q^2, M^2\xi^2; m(Q^2), 0, 0) \\
& - \big(m_i + 4m(Q^2) + M\xi\big).
\end{aligned} \tag{A.4}$$

$$\begin{aligned}
\mathrm{F4} =\, & 2i\Bigg(2\big[M\xi - m(Q^2)\big]\mathbf{B}_0(M^2\xi^2; m(Q^2), 0) + 2\big[m_i - m(Q^2)\big]\mathbf{B}_0(m_i^2; m(Q^2), 0) \\
& + 2\big[m_i + 2m(Q^2) + M\xi\big]\mathbf{B}_0(-Q^2; 0, 0) + 2m_i\,\mathbf{B}_1(m_i^2; m(Q^2), 0) + 2M\xi\,\mathbf{B}_1(M^2\xi^2; m(Q^2), 0) \\
& + 2\big[2m^3(Q^2) + m_i m^2(Q^2) + M\xi m^2(Q^2) - M\xi m_i^2 - M^2\xi^2 m_i - 2M\xi m_i m(Q^2) - m(Q^2)Q^2\big] \\
& \mathbf{C}_0(m_i^2, -Q^2, M^2\xi^2; m(Q^2), 0, 0) + 2\big[2m_i m(Q^2) - M^2\xi^2 - 2M\xi\, m(Q^2) + m_i^2\big] \\
& \big(m_i\,\mathbf{C}_1(m_i^2, -Q^2, M^2\xi^2; m(Q^2), 0, 0) - M\xi\,\mathbf{C}_2(m_i^2, -Q^2, M^2\xi^2; m(Q^2), 0, 0)\big) - 3(m_i + M\xi)\Bigg).
\end{aligned} \tag{A.5}$$

The function $m(Q^2)$ represents the running of the quark mass in the loop. We used the RunDec package [25] for the computation of the quark masses at different energy scales. The standard notation for the Passarino-Veltman loop functions is employed.

We use Package-X [30] to analytically evaluate the loop integrals, and the CollierLink extension —that uses the COLLIER library [40]— to numerically evaluate the Passarino-Veltman functions.

Acknowledgements

F. F. is grateful to Conacyt for funding. It is my pleasure to thank Alejandro Ibarra, Xabier Marcano, Marcela Marín and Pablo Roig for a fruitful collaboration and insightful discussions.

---

i. The running of these Wilson coefficients between the invariant mass of the nuclei conversions and the decaying lepton mass scale, that corresponds to their determination in Eqs. (13), is neglected. This small effect will not change our results and conclusions.

ii. The validity of our EFT in these processes is addressed at the end of this section.

1. F. Fortuna *et al.*, Indirect upper limits on $\ell\mathbf{i} \to \ell\mathbf{j}\gamma\gamma$ from $\ell\mathbf{i} \to \ell\mathbf{j}\gamma$, *Phys. Rev. D* **107** (2023) 015027, `https://doi.org/10.1103/PhysRevD.107.015027`.
2. J. D. Bowman *et al.*, New Upper Limit for $\mu \to e\gamma\gamma$, *Phys. Rev. Lett.* **41** (1978) 442, `https://doi.org/10.1103/PhysRevLett.41.442`.
3. S. Davidson *et al.*, Probing $\mu e\gamma\gamma$ contact interactions with $\mu \to e$ conversion, *Phys. Rev. D* **102** (2020) 115043, `https://doi.org/10.1103/PhysRevD.102.115043`.
4. A. Gemintern *et al.*, Lepton flavor violating decays $L \to \ell\gamma\gamma$ as a new probe of supersymmetry with broken R parity, *Phys. Rev. D* **67** (2003) 115012, `https://link.aps.org/doi/10.1103/PhysRevD.67.115012`.
5. A. Cordero-Cid, G. Tavares-Velasco, and J. J. Toscano, Implications of a very light pseudoscalar boson on lepton flavor violation, *Phys. Rev. D* **72** (2005) 117701, `https://doi.org/10.1103/PhysRevD.72.117701`.
6. J. I. Aranda *et al.*, Higgs mediated lepton flavor violating tau decays $\tau \to \mu$ gamma and $\tau \to \mu\gamma\gamma$ in effective theories, *Phys. Rev. D* **78** (2008) 017302, `https://link.aps.org/doi/10.1103/PhysRevD.78.017302`.
7. J. I. Aranda *et al.*, Effective Lagrangian description of Higgs mediated flavor violating electromagnetic transitions: Implications on lepton flavor violation, *Phys. Rev. D* **79** (2009) 093009, `https://doi.org/10.1103/PhysRevD.79.093009`.
8. D. A. Bryman, S. Ito, and R. Shrock, Upper limits on branching ratios of the lepton-flavor-violating decays $\tau \to \ell\gamma\gamma$ and $\tau \to \ell X$, *Phys. Rev. D* **104** (2021) 075032, `https://doi.org/10.1103/PhysRevD.104.075032`.
9. A. M. Baldini *et al.*, Search for the lepton flavour violating decay $\mu^+ \to e^+\gamma$ with the full dataset of the MEG experi-

ment, *Eur. Phys. J. C* **76** (2016) 434, https://doi.org/10.1140/epjc/s10052-016-4271-x.

10. D. Grosnick *et al*., Search for the Rare Decay $\mu^+ \to e^+\gamma\gamma$, *Phys. Rev. Lett*. **57** (1986) 3241, https://doi.org/10.1103/PhysRevLett.57.3241.
11. B. Aubert *et al.*, Searches for Lepton Flavor Violation in the Decays $\tau^+ \to e^+-$ gamma and $\tau^+ \to mu^+-$ gamma, *Phys. Rev. Lett.* **104** (2010) 021802, https://link.aps.org/doi/10.1103/PhysRevLett.104.021802.
12. A. Abdesselam *et al*., Search for lepton-flavor-violating taulepton decays to $\ell\gamma$ at Belle, *JHEP* **10** (2021) 19, https://doi.org/10.1007/JHEP10(2021)019.
13. I. Angelozzi, In pursuit of lepton flavour violation: A search for the $\tau \to \mu\gamma\gamma$ decay with ATLAS at $\sqrt{s} = 8$ TeV, Ph.D. thesis, U. Amsterdam, IHEF (2017).
14. W. Bertl *et al*., A Search for muon to electron conversion in muonic gold, *Eur. Phys. J. C* **47** (2006) 337, https://doi.org/10.1140/epjc/s2006-02582-x.
15. S. Gninenko *et al*., Deep inelastic $e-\tau$ and $\mu-\tau$ conversion in the NA64 experiment at the CERN SPS, *Phys. Rev. D* **98** (2018) 015007, https://doi.org/10.1103/PhysRevD.98.015007.
16. S. Banerjee *et al*., Snowmass 2021 White Paper: Charged lepton flavor violation in the tau sector (2022), https://doi.org/10.48550/arXiv.2203.14919.
17. R. D. Bolton *et al*., Search for Rare Muon Decays with the Crystal Box Detector, *Phys. Rev. D* **38** (1988) 2077, https://doi.org/10.1103/PhysRevD.38.2077.
18. V. N. Gribov and L. N. Lipatov, Deep inelastic e p scattering in perturbation theory, *Sov. J. Nucl. Phys.* **15** (1972) 438.
19. Y. L. Dokshitzer, Calculation of the Structure Functions for Deep Inelastic Scattering and e+ e- Annihilation by Perturbation Theory in Quantum Chromodynamics., *Sov. Phys. JETP* **46** (1977) 641.
20. G. Altarelli and G. Parisi, Asymptotic Freedom in Parton Language, *Nucl. Phys. B* **126** (1977) 298, https://doi.org/10.1016/0550-3213(77)90384-4.
21. K. Kovarik *et al*., nCTEQ15 - Global analysis of nuclear parton distributions with uncertainties in the CTEQ framework, *Phys. Rev. D* **93** (2016) 085037, https://link.aps.org/doi/10.1103/PhysRevD.93.085037.
22. D. B. Clark, E. Godat, and F. I. Olness, ManeParse: A Mathematica reader for Parton Distribution Functions, *Comput. Phys. Commun.* **216** (2017) 126, https://doi.org/10.1016/j.cpc.2017.03.004.
23. F. Fortuna, et al., Lepton Flavor Violation from diphoton effective interactions (2023), https://arxiv.org/abs/2305.04974.
24. T. Husek, K. Monsalvez-Pozo, and J. Portoles, Lepton-flavour violation in hadronic tau decays and $\mu-\tau$ conversion in nuclei, *JHEP* **01** (2021) 059, https://doi.org/10.1007/JHEP01(2021)059.
25. R. Kitano, M. Koike, and Y. Okada, Detailed calculation of lepton flavor violating muon electron conversion rate for various nuclei, *Phys. Rev. D* **66** (2002) 096002, https://link.aps.org/doi/10.1103/PhysRevD.66.096002.
26. T. Suzuki, D. F. Measday, and J. P. Roalsvig, Total Nuclear Capture Rates for Negative Muons, *Phys. Rev. C* **35** (1987) 2212, https://doi.org/10.1103/PhysRevC.35.2212.
27. L. Bartoszek *et al*., Mu2e Technical Design Report (2014), https://doi.org/10.2172/1172555.
28. R. Abramishvili *et al*., COMET Phase-I Technical Design Report, *PTEP* **2020** (2020) 033C01, https://doi.org/10.1093/ptep/ptz125.
29. P. W. Cattaneo and A. Schöning, MEG II and Mu3e status and plan, *EPJ Web Conf*. **212** (2019) 01004, https://doi.org/10.1051/epjconf/201921201004.
30. Y. Kuno *et al*., An Experimental Search for a $\mu^- - e^-$ Conversion at Sensitivity of the Order of 10^{-18} with a Highly Intense Muon Source: PRISM (2006), https://j-parc.jp/researcher/Hadron/en/pac_0606/pdf/p20-Kuno.pdf.
31. M. Moritsu, Search for Muon-to-Electron Conversion with the COMET Experiment, *Universe* **8** (2022) 196, https://doi.org/10.3390/universe8040196.
32. A. Deshpande, Physics of an Electron Ion Collider, *Nucl. Phys. A* **904-905** (2013) 302c, https://doi.org/10.1016/j.nuclphysa.2013.01.076.
33. J.-P. Delahaye *et al*., Enabling Intensity and Energy Frontier Science with a Muon Accelerator Facility in the U.S.: A White Paper Submitted to the 2013 U.S. Community Summer Study of the Division of Particles and Fields of the American Physical Society, In Snowmass 2013: Snowmass on the Mississippi (2013), https://doi.org/10.48550/arXiv.1308.0494.
34. Y. C. Acar *et al*., Future circular collider based lepton-hadron and photon-hadron colliders: Luminosity and physics, *Nucl. Instrum. Meth. A* **871** (2017) 47, https://doi.org/10.1016/j.nima.2017.07.041.
35. H. Baer, et al., The International Linear Collider Technical Design Report - Volume 2: Physics (2013), https://doi.org/10.48550/arXiv.1306.6352.
36. M. Sher and I. Turan, $\mu+N \to \tau+N$ at a muon or neutrino factory, *Phys. Rev. D* **69** (2004) 017302, https://doi.org/10.1103/PhysRevD.69.017302.
37. S. Kanemura *et al*., A Study of lepton flavor violating $\mu N(eN) \to \tau X$ reactions in supersymmetric models, *Phys. Lett. B* **607** (2005) 165, https://doi.org/10.1016/j.physletb.2004.12.038.
38. A. Abada, et al., In-flight cLFV conversion: $e-\mu$, $e-\tau$ and $\mu-\tau$ in minimal extensions of the standard model with sterile fermions, *Eur. Phys. J. C* **77** (2017) 304, https://doi.org/10.1140/epjc/s10052-017-4864-z.
39. M. Takeuchi, Y. Uesaka, and M. Yamanaka, Higgs mediated CLFV processes $\mu N(eN) \to \tau X$ via gluon operators, *Phys. Lett. B* **772** (2017) 279, https://doi.org/10.1016/j.physletb.2017.06.054.
40. E. Ramirez and P. Roig, Lepton flavor violation within the simplest little Higgs model, *Phys. Rev. D* **106** (2022) 056018, https://link.aps.org/doi/10.1103/PhysRevD.106.056018.

41. B. Grzadkowski, *et al*., Dimension-Six Terms in the Standard Model Lagrangian, *JHEP* **10** (2010) 085, https://doi.org/10.1007/JHEP10(2010)085.

42. W. Buchmüller and D.Wyler, Effective Lagrangian Analysis of New Interactions and Flavor Conservation, *Nucl. Phys. B* **268** (1986) 621, https://doi.org/10.1016/0550-3213(86)90262-2.

43. S. N. Gninenko *et al*., Probing lepton flavor violation in muon-neutrino $+N \rightarrow \tau+$ scattering and $\mu \rightarrow \tau$ conversion on nucleons, *Mod. Phys. Lett. A* **17** (2002) 1407, https://doi.org/10.1142/S0217732302007855.